PCCP

Accepted Manuscript

ROYAL SOCIETY OF CHEMISTRY

www.rsc.org/pccp

Cite this: DOI: 10.1039/c0xx00000x

www.rsc.org/xxxxxx

ARTICLE TYPE

Theoretical study of three gas-phase reactions involving the production or loss of methane cations

Leonardo Baptista[a*] and Enio F. da Silveira[b]

Received (in XXX, XXX) Xth XXXXXXXXX 20XX, Accepted Xth XXXXXXXXX 20XX

DOI: 10.1039/b000000x

Hydrocarbon ions are important species in flames, spectroscopy and the interstellar medium. Their importance is reflected in the extensive body of literature on the structure and reactivity of carbocations. However, the geometry, electronic structure and reactivity of carbocations are difficult to assess. This study aims to contribute to current knowledge of this subject by presenting a quantum mechanics description of methane cation dissociation using multiconfigurational methods. The geometric and electronic parameters of the minimum structure were determined for three main reaction paths: the dissociation $CH_4^+ \rightarrow CH_2^+ + H_2$ and the dissociation/recombination processes $CH_4^+ \leftrightarrow CH_3^+ + H$. The electronic and energetic effects of these reactions were analyzed, and it was found that each reaction path has a strong dependence on the methodology used as well as a strong multiconfigurational character during dissociation. The first doublet excited states are inner-shell excited states and may correspond to the ions that are expected to be formed after electron detachment. The rate coefficient for each reaction path was determined using variational transition state theory and RRKM/master equation calculations. The major dissociation paths, with their rate coefficients at the high-pressure limit, are: $CH_4^+(\tilde{X}\ ^2B_1) \rightarrow CH_3^+(A\ ^2A_1') + H(\ ^2S)$ ($k_\infty(T) = 1.42\times10^{+14}$ s^{-1} exp(-37.12/RT)) and $CH_4^+(\tilde{X}\ ^2B_1) \rightarrow CH_2^+(A\ ^2A_1) + H_2(\ ^2\Sigma_g^+)$ ($k_\infty(T) = 9.18\times10^{+14}$ s^{-1} exp(-55.77/RT)). Our findings help to explain the abundance of ions formed from CH_4 in the interstellar medium and to build models of chemical evolution.

Introduction

Methane is the smallest hydrocarbon, making it of great importance in industry and its occurrence in the environment and interstellar medium of particular significance. In the environment, methane acts as a greenhouse gas and has a direct impact on the Earth's climate; in the interstellar medium, it are observed, for example, in star-forming and protoplanetary regions and in icy comets[1–5]; and in industry and vehicles it is used as fuel[6,7], and as a precursor for large molecules and in the synthesis of diamonds by vapor deposition[8,9]. Because of the large number of applications in which it is used, neutral methane has been the subject of various kinetic studies[10–14].

Ionized methane also appears in many phenomena and can be found, for instance, in the interstellar medium as a result of the absorption of UV or X-ray radiation or the impact of cosmic rays[15–18]. In the terrestrial environment, it occurs in combustion processes because of the high temperature in flames (some ions observed in flames may be produced as a result of the dissociation of CH_4^+)[19] or during the activation of hydrocarbons in the petroleum and natural gas industry[20]. After ionization, the CH_4 tetrahedral structure is distorted by the Jahn-Teller effect into a C_{2v} geometry[21]. This effect is observed in photoionization spectra, providing an unexpected and complex vibrational pattern[20,22–25]. Also, the same effect has been invoked to explain the photoelectron spectra of methane: a rigorous theoretical analysis by Mondal and Varandas[23] of the first photoelectron band of methane successfully described the observed vibrational pattern.

The potential energy surface (PES) of the methane cation and its vibrational structure has been widely explored[20,22,25]. It is well established that the minimum structure has C_{2v} symmetry, but the region of the PES near the minimum is flat and presents several local minima and saddle points[26,27,25]. Much effort has been dedicated to describing the geometry of CH_4^+ in terms of Jahn-Teller distortion and to using the CH_4^+ structure to model this effect [21,23,26–30].

The formation of complex molecules, such as amino acids, from the irradiation of astrophysical ices in the interstellar medium seems to be a promising source of data on astrochemical processes[31,32,33]. Using 6 MeV $^{16}O^{2+}$, 220 MeV $^{16}O^{7+}$, 267 MeV $^{56}Fe^{22+}$ and 606 MeV $^{70}Zn^{26+}$ ion beams impacting on solid methane, Mejía and de Barros[18,16] investigated the radiolysis of methane ice by fast heavy ions and subsequent synthesis of new molecular species with two and three carbon atoms. Previously, Libby radiolysed solid methane in liquid argon at 77 K using γ-rays[34,35] and observed the polymerization of methane and formation of polycondensates with an average molecular formula of $C_{20}H_{40}$. These studies show that the ionization of methane synthesizes hydrocarbons with more than two carbon atoms[20].

The high energy of projectile ions impacting on CH_4 ice is believed to prompt electronic excitation and ionization of

Table 1. Geometric parameters. Bond distances are in angstroms and bond angles in degrees.

	rC-H(2)	rC-H(3)	rC-H(4)	rC-H(5)	θH(2)CH(5)	θH(3)CH(4)
CAS(5,6)/6-31G**	1.197	1.094	1.074	1.195	52.6	126.5
CAS(5,6)/6-311G**	1.204	1.095	1.074	1.202	53.0	126.7
NEVPT2(5,6)/6-31G**	1.183	1.084	1.078	1.181	54.0	125.9
NEVPT2(5,6)/6-311G**	1.193	1.088	1.082	1.192	54.7	126.1
CAS(7,8)/6-31G**	1.197	1.096	1.096	1.197	53.3	126.5
CAS(7,8)/6-311G**	1.204	1.096	1.096	1.204	53.6	126.6
NEVPT2(7,8)/6-31G**	1.182	1.085	1.085	1.182	53.8	125.8
NEVPT2(7,8)/6-311G**	1.192	1.089	1.089	1.193	54.6	126.1
CAS(7,8)/6-311G(2df,2pd)	1.202	1.093	1.093	1.202	53.5	126.7
NEVPT2(7,8)/6-311G(2df,2pd)	1.187	1.083	1.083	1.187	54.5	126.2
CAS(7,8)/cc-pvqz	1.202	1.092	1.092	1.203	53.3	126.9
NEVPT2(7,8)/cc-pvqz	1.185	1.185	1.081	1.081	54.5	126.1

methane, followed by its dissociation and the formation of new molecular species, as well as the sputtering of several ionic and neutral species. The products thus formed or emitted can be expected to be directly related to the CH_4^+ fragments and other molecular species generated after the impact.

Methane and other hydrocarbons observed in the interstellar medium[2,4] interact with high-energy particles or the solar wind or absorb X-rays, leading to ionization/dissociation processes. The study of the reactivity of the ions formed in these processes may elucidate several mechanisms in the interstellar medium and help improve our understanding of the chemical evolution of planetary atmospheres.

Likewise, the study of the dissociation pathways of the methane cation is important not only for an understanding of the transformations undergone by methane in the interstellar medium after ionization (in particular so that kinetic parameters can be determined to build kinetic models), but also for modeling several effects observed in the dissociation and recombination of ions in the gas phase.

Computational details

The electronic structure of the ground state of the methane cation and its dissociation/recombination pathways, including those related to excited states, were investigated by multiconfigurational and coupled cluster methods with 6-31G(d,p), 6-311G(d,p), 6-311G(2df,2pd) and cc-pvQZ basis sets. The active spaces chosen were CAS(5,6) (five electrons and six orbitals) and CAS(7,8) (seven electrons and eight orbitals). Dynamic correlation was included in the CAS method by using n-electron valence state perturbation theory (NEVPT2)[36,37] and multireference correlation interaction with singles and doubles (MRCISD). For those methods for which analytical gradients are not available, the optimization procedures and energy evaluation used the numerical gradients calculated by the quantum chemical package.

The geometry of the ground state was optimized without any geometrical constraint, and the harmonic vibrational frequencies were determined to establish whether the structure found corresponded to a minimum on the potential energy surface. The study included dissociation of the methane cation by stretching of the C-H(2) bond (bond distance between carbon and hydrogen number 2) and a recombination reaction between a hydrogen atom and CH_3^+ to form CH_4^+. All dissociation paths were obtained by relaxed scan along the proper bond length. The dissociation/recombination reactions were evaluated by multiconfigurational and coupled cluster methods. The changes in energy, electronic configuration and excited states along the reaction path were analyzed at the MRCISD(7,8)/6-311G(d,p) level with the geometries optimized at the NEVPT2(7,8)/6-311G(2df,2pd) level [MRCISD(7,8)/6-311G(d,p)//NEVPT2(7,8)/6-311G(2df,2pd) method]. Because of the lack of experimental data, the results were refined with the MRCISD and CCSD(T) methodologies to provide a reliable ensemble of electronic structure data. All electronic structure investigation was performed with the Orca 2.9.1 package[38,39].

The rate coefficients of thermal dissociation/recombination were determined in two different ways: (i) by applying canonical variational transition state theory (CVTST) maximizing activation free energy along the reaction paths at 1.0 atm and different temperatures; and (ii) by determining the sum and density of states along the reaction paths followed by minimization of the sum of states to find the variational transition structure. The density and sum of states were calculated with DenSum code supplied with the Multiwell[40,41] package, and the location of the transition structure was identified using external spreadsheet software. The sum of states and angular momentum, for both dissociation reactions, were plotted in function of bond distance and the molecular configuration that minimizes the sum of states identified. The microcanonical variational transition-state theory (μVTST) rate coefficients were calculated using RRKM theory[42–48], and centrifugal corrections were included by averaging k(E,J) over a thermal distribution of angular momentum J. The high-pressure rate coefficients, k_∞, were obtained by averaging the μVTST coefficients over a Boltzmann distribution. The Arrhenius parameters were determined by both methods.

Next, the master equation was solved to estimate the rate coefficients in the pressure fall-off and determine their dependency on the energy transfer function for a population with a Maxwell-Boltzmann distribution and the calculated μVTST rate coefficients. The Lennard-Jones parameters used to determine the collision frequency between methane cations and an inert gas (Ar) were obtained from Miller's master equation study for the dissociation of methane[12]. Lennard-Jones parameterization for neutral methane was considered a suitable approach for an initial study. Following the earlier study by Brown and Miller[12,49], the evaluation of the energy transfer function uses the double exponential model [Equation (a)] and the 0.1/10 approach. In this

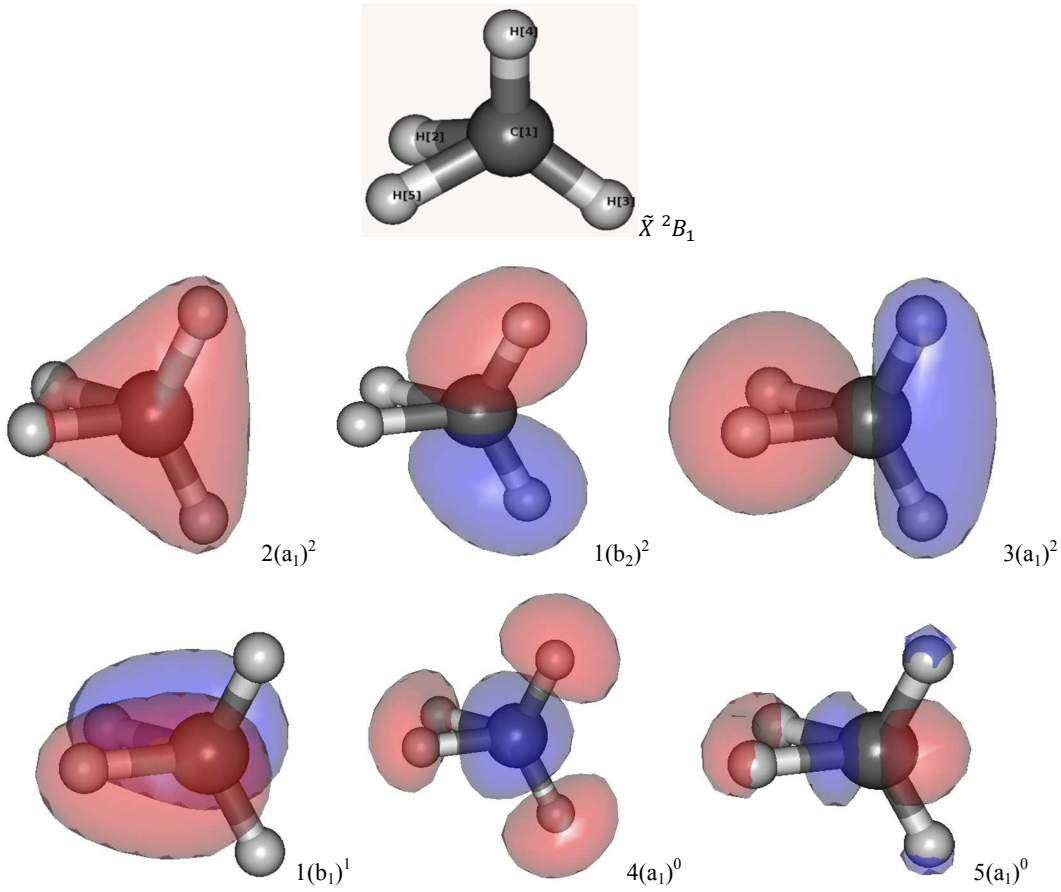

Fig. 1. Geometry and molecular orbitals of the methane cation ground state optimized at the CAS(7,8)/cc-pvQZ level. The inner shell is not shown in this figure

model, the parameters related to the energy transferred per deactivation collision[12,50,51], α_1 and α_2, were considered independent of temperature. The 0.1/10 approach uses $\alpha_2 = 10\alpha_1$ and $f = 0.1$. For the purposes of comparison, an exponential decay function is considered to model the energy transfer function, as in Equation (b).

$$P(E,E') = \frac{1}{C_N(E')}\left[(1-f)\exp\left(-\frac{\Delta E}{\alpha_1}\right) + f\exp\left(-\frac{\Delta E}{\alpha_2}\right)\right] \quad E \le E' \text{(a)}$$

$$P(E,E') = \frac{1}{C_N(E')}\exp\left(-\frac{\Delta E}{\alpha}\right) \quad E \le E' \qquad \text{(b)}$$

Again, because of the lack of experimental data, the parameter α was varied in the range 50 cm^{-1} to 500 cm^{-1} and the final results were analyzed. The thermal energy distribution was used to describe the initial energy of the reactants and to calculate the unimolecular rate coefficient using Ar as collider. The master equation was solved simultaneously for the three processes (reactions 1 to 3) analyzed here. The Multiwell[40,41,52] package developed by Barker et al. was used to solve the master equation.

Results and Discussion

Geometry and Electronic Structure

Singly ionized methane has nine electrons. As shown in Figure 1 and Table 1 (which gives the most important geometrical parameters determined by multiconfigurational methods), this cation has C_{2v} symmetry and two pairs of equivalent hydrogens. The results in Table 1 show that the choice of five electrons and six orbitals as active space leads to a small deviation in the C_{2v} symmetry, where the four C-H bonds are not exactly equal to each other. In fact, the effect of removing one electron is that the rC-H(2) and rC-H(5) bonds are nearly 9% longer than the rC-H(3) and rC-H(4) bonds. After ionization, one of the methane bond angles becomes smaller to compensate for removal of the electron, changing the neutral methane tetrahedral symmetry into C_{2v} symmetry. As expected, removal of an electron from a bond increases the bond lengths rC-H(2) and rC-H(5)[28]. At the CAS(7,8)/cc-pvQZ level, the electronic configuration of the CH_4^+ ground state is $2(a_1)^2\ 1(b_2)^2\ 3(a_1)^2\ 1(b_1)^1$, which leads to the $\tilde{X}\ ^2B_1$ electronic state (Figure 1). The two first unoccupied orbitals have A_1 symmetry and an anti-bonding character. At the MRCISD(7,8)/6-311G(d,p)//NEVPT2(7,8)/6-311G(2df,2pd) level, a change in orbital ordering is observed: the method predicts the $2(a_1)^2\ 3(a_1)^2\ 1(b_2)^2\ 1(b_1)^1$ electronic configuration for the ground state and B_1 symmetry for the second unoccupied orbital. In agreement with previous theoretical studies, we failed to find other minimum-energy structures with symmetry other than C_{2v}[25,28].

Table 2. Dissociation energies determined using multiconfigurational methods. All values are in kcal mol^{-1}

Level	Reaction 1	Reaction 3
CAS(5,6)/6-31G(d,p)	46.04	24.13
CAS(5,6)/6-311G(d,p)	47.45	24.21
NEVPT2(5,6)/6-31G(d,p)	59.69	59.63
NEVPT2(5,6)/6-311G(d,p)	60.69	33.78
NEVPT2(7,8)/6-31G(d,p)	58.88	25.01
NEVPT2(7,8)/6-311G(d,p)	60.26	39.13
NEVPT2(7,8)/6-311G(2df,2pd)	64.35	42.04
NEVPT2(7,8)/cc-pvQZ	65.30	40.04
MRCISD(5,6)/6-31G(d,p)//CAS(5,6)/6-31G(d,p)	57.19	33.93
MRCISD(5,6)/6-311G(d,p)//CAS(5,6)/6-31G(d,p)	58.11	38.44
MRCISD(7,8)/6-311G(d,p)//NEVPT2(7,8)/6-311G(2df,2pd)	58.04	38.32

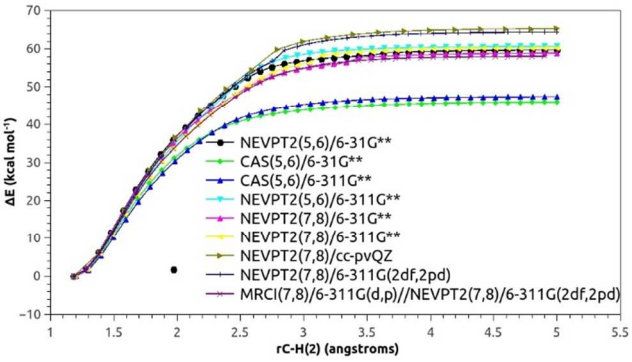

(a)

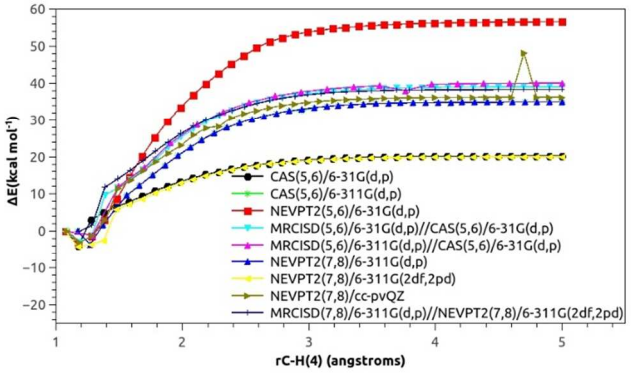

(b)

Fig. 2. Possible dissociation pathways of the methane cation; (a) $CH_4^+ \rightarrow CH_2^+ + H_2$ reaction; (b) $CH_3^+ + H \leftrightarrow CH_4^+$ reaction.

Dissociation curves for the ground state

Correctly describing CH_4^+ dissociation is a challenging task as the existence of two pairs of equivalent hydrogen atoms generates two different dissociation pathways. We found that the predicted reaction pathways are very sensitive to the methodology used. We therefore investigated the following two channels in detail: (i) the dissociation of CH_4^+ following reaction 1 below, and (ii) the gas-phase recombination/dissociation of a methyl cation with a hydrogen atom to produce CH_4^+, following reactions 2 and 3.

$$CH_4^+ \rightarrow CH_2^+ + H_2 \quad (1)$$

$$CH_3^+ + H \rightarrow CH_4^+ \quad (2)$$

$$CH_4^+ \rightarrow CH_3^+ + H \quad (3)$$

Reaction 1 is observed after stretching of the C-H(2) or C-H(5) bond. Analysis of configuration state functions (CSF) at the MRCISD(7,8)/6-311G(d,p)//NEVPT2(7,8)/6-311G(2df,2pd) level indicates the formation of the CH_2^+ doublet radical cation and a neutral hydrogen molecule. The dissociation curves for this reaction are shown in Figure 2a. As expected, increasing the basis set and the active space decreases the energy of the potential energy curve.

The CAS result is highly dependent on the basis set and active space. Reaction 1 is obtained independently of basis set if five electrons and six orbitals are considered as active space. However, increasing the active space causes the methane cation to dissociate into planar CH_3^+ and a hydrogen atom. Increasing the basis set does not change the CAS(7,8) qualitative prediction, i.e., the methane cation always dissociates into $CH_3^+ + H$ (reaction 3). To resolve this issue dynamic correlation was included by using perturbation treatment (NEVPT2 method) or a multireference configuration interaction method (MRCISD). All the NEVPT2 and MRCISD results led to reaction 1 independently of the active space and basis set. In contrast, the CCSD and CCSD(T) methods, shown in the Supplementary Information Section, always predicted that stretching of the C-H(2) or C-H(5) bond would follow reaction 3.

A description of the formation of $CH_3^+ + H$ is essential to elucidate all possible dissociation products and determine which methodology provides the correct and best description of the dissociation pathways. Attempts to stretch the C-H(3) or C-H(4) bonds using multiconfigurational methods in order to produce reaction 3 failed because of the jump discontinuity observed in the curves obtained (available in the Supplementary Information Section). Each side of the discontinuity refers to different dissociation pathways and may be related to the crossing of two different electronic states.

At the CCSD(T)/6-311G(d,p) level, dissociation of the C-H(4) bond follows the reaction $CH_4^+ \rightarrow CH_3 + H^+$, with a dissociation energy of 99.4 kcal mol^{-1}. Prediction of these products by the coupled-cluster method provides a partial answer to the problematic evaluation of C-H(4) dissociation by multiconfigurational methods: (1) the multiconfigurational character of bond breaking is not taken into account by the coupled cluster method[53], while the CAS and NEVPT2 methodology does take this effect into account; and (2) the CAS wavefunction is obtained by using a configuration interaction procedure in the active space associated with a molecular orbital

optimization. This procedure searches for a minimum energy electronic configuration for several electronic states. Based on this, in the first stages of the dissociation reaction the method leads to the $CH_3 + H^+$ configuration. Near 2 Å, where the jump discontinuity occurs, the CAS and NEVPT2 methods generate the $CH_3^+ + H$ configuration, and the dissociation of CH_4^+ finishes with these products. The discontinuity observed in the potential energy curve is caused by the transition from a high energy configuration ($CH_3 + H^+$) to a lower energy configuration ($CH_3^+ + H$). Indeed, the coupled-cluster method predicts the dissociation of CH_4^+ into high-energy products.

The breaking of the C-H(3) or C-H(4) bond involves changes in the inner shell $1b_2$ and $3a_1$ orbitals, which produce an abrupt increase in dissociation energy along the reaction coordinate. Near 2 Å the CAS method finds a lower-energy electronic configuration which flips the order of the orbitals and results in the discontinuity in the dissociation curve. We also observed that near 2 Å, before the jump discontinuity, two high-order excited states contribute to the ground state energy: the |22012> configuration and, to a lesser extent, the |22111> configuration. However, some questions remain. Firstly, is it necessary to include vibronic coupling to obtain the right description of C-H(4) bond-breaking?[23] And, secondly, does a state-averaged CASSCF procedure lead to the expected products? These issues are currently under analysis by this research group.

The multiconfigurational results were chosen to predict the right dissociation products in light of two facts: (1) the significant multiconfigurational character observed along the bond dissociation curve; and (2) the fact that the dissociation energy of the $CH_4^+ \rightarrow CH_3 + H^+$ reaction is greater than 90 kcal mol^{-1}, whereas the dissociation energy corresponding to reaction 3 is in the 30 to 40 kcal mol^{-1} range.

To investigate how planar CH_3^+ and an H atom are formed (reaction 3), the dynamics of these two species was studied in a recombination reaction. The potential energy curves for this approach are shown in Figure 2. The CSF analysis of the starting configuration, at the MRCISD(7,8)/6-311G(d,p)//NEVPT2(7,8)/6-311G(2df,2pd) level, shows eight electrons in the CH_3^+ fragment, indicating a monocation species, and one in the hydrogen, confirming that reaction 2 starts with the right electronic configuration. The distance between these two fragments was varied from 5.0 Å to 1.08 Å. Near 1.4 Å, the hydrogen atom starts to interact with the carbon atom and binds to it, taking the position of the H(2) atom. The final structure is the methane cation with C_{2v} symmetry.

Dissociation reactions 1 and 3 show that the dissociation energy seems to govern the competition between the two dissociation channels. Table 2 shows the dissociation energy without ZPE correction determined by the multiconfigurational methods. The following behaviors were observed: (1) in almost every case, the increase in the basis set increases the dissociation energy. The major deviations in this behavior were observed for reaction 3. At the NEVPT2(5,6)/6-31G(d,p) and NEVPT2(5,6)/6-311G(d,p) levels this deviation may be related to the chosen active space. At the NEVPT2(5,6)/6-311G(2df,2pd) and NEVPT2(7,8)/cc-pvQZ levels the change in the basis set style, size and number of polarization functions could be responsible for the observed deviation; (2) inclusion of dynamic correlation increases the dissociation energy; (3) changing the active space causes a small modification in the dissociation energy. An exception is observed for reaction 3 at the NEVPT2(5,6)/6-31G(d,p) and NEVPT2(5,6)/6-31G(d,p) levels, where the dissociation energy changes by 34.6 kcal mol^{-1} because of the increased active space; and (4) from the thermochemical point of view, the dissociation into $CH_3^+ + H$ is the most favorable pathway, and the energy difference between the two dissociation channels is nearly 20 kcal mol^{-1} in the major levels of theory. Analysis of the dissociation paths and dissociation energies shows that reaction 3 is very sensitive to the level of theory applied.

The most reliable and precise method used in this study is the MRCISD(7,8)/6-311G(d,p)//NEVPT2(7,8)/6-311G(2df,2pd) method. We therefore consider the dissociation energies calculated at this level to be more accurate.

Dissociation curves for the excited states

The transition energies calculated at the MRCISD(7,8)/6-311G(d,p)//NEVPT2(7,8)/6-311G(2df,2pd) level are shown in Table 3. All doublet excited states are for inner shell singly occupied molecular orbitals and are energetically substantially above the dissociation energies calculated. The inner shell excited states (A^2B_2 and A^2A_1) represent the electronic configuration of different monopositive ions produced after the impact of the projectile. Examination of the dissociation curves for the A^2B_2 and A^2A_1 states provides the dissociation products of these different ions.

Table 3. Transition energies evaluated at the MRCISD(7,8)/6-311G(d,p)//NEVPT2(7,8)/6-311G(2df,2pd) level.

Configuration	State	Transition energy (eV)
$2(a_1)^2\ 3(a_1)^2\ 1(b_2)^2\ 1(b_1)^1$	$\tilde{X}\ ^2B_1$	0.000
$2(a_1)^2\ 3(a_1)^2\ 1(b_2)^1\ 1(b_1)^2$	A^2B_2	4.579
$2(a_1)^2\ 3(a_1)^1\ 1(b_2)^2\ 1(b_1)^2$	A^2A_1	5.688
$2(a_1)^2\ 3(a_1)^2\ 1(b_2)^1\ 1(b_1)^1\ 4(a_1)^1$	a^4A_2	12.228

The dissociation curves, including those for the excited states, are shown in Figure 3. Excitation of the $\tilde{X}\ ^2B_1 - a^4A_2$ transition leads to a repulsive state that contributes to the molecular dissociation in both processes analyzed. The dissociation products corresponding to the C-(2) bond stretching (Figure 3a) in the a^4A_2 curve have the configuration 0.9085|22111>, very similar to that obtained in the recombination curve (Figure 3b) for the same state, 0.8984|22111> + 0.0191|21211>.

The potential energy curves for C-(2) bond-stretching (Figure 3a) have a conical intersection between states A^2A_1 and a^4A_2 at 1.9 Å and an avoided crossing between the A^2B_2 and A^2A_1 curves at 1.5 Å. Dissociation along the $\tilde{X}\ ^2B_1$, A^2A_1 and a^4A_2 curves forms H_2 and CH_2^+, but in distinct electronic states, and dissociation along the A^2B_2 state forms the ground state of neutral CH_2 and the H_2^+ cation in the Σ_g^+ state.

Dissociation according to reaction 3 through states A^2A_1 and a^4A_2 leads to the excited state of the CH_3^+ ion and the neutral H atom; the only difference is the multiplicity of CH_3^+ formed in each dissociation process. Analysis of CSF indicates that the A^2B_2 state dissociates into a CH_3 radical and H^+.

Table 4. Kinetic parameters at the high-pressure limit for the dissociation/recombination reactions of CH_4^+ using the electronic structure data evaluated at the MRCISD(7,8)/6-311G(d,p)//NEVPT2(7,8)/6-311G(2df,2pd) level. The rate coefficients of the dissociation reactions are in s^{-1}, the pre-exponential factors (A factor) in s^{-1} and the activation energy in kcal mol^{-1}. The rate coefficients of the recombination reaction and the A factor are in cm^3 $molecule^{-1}$ s^{-1}

	Reaction 1		Reaction 2		Reaction 3	
T	CVTST	$k_{\infty,diss}$	CVTST	$k_{\infty,rec}$	CVTST	$k_{\infty,diss}$
273	1.19×10^{-35}	2.12×10^{-31}	1.61×10^{-11}	6.96×10^{-09}	6.29×10^{-19}	2.71×10^{-16}
298.15	1.63×10^{-31}	1.21×10^{-27}	2.72×10^{-11}	7.02×10^{-09}	3.36×10^{-16}	8.70×10^{-14}
310	8.50×10^{-30}	4.41×10^{-26}	3.43×10^{-11}	7.15×10^{-09}	4.58×10^{-15}	9.54×10^{-13}
330	3.56×10^{-27}	1.06×10^{-23}	4.84×10^{-11}	7.24×10^{-09}	2.46×10^{-13}	3.68×10^{-11}
380	8.11×10^{-22}	7.62×10^{-19}	1.05×10^{-10}	7.80×10^{-09}	8.52×10^{-10}	6.34×10^{-08}
400	4.77×10^{-20}	3.07×10^{-17}	1.33×10^{-10}	7.82×10^{-09}	1.25×10^{-08}	7.40×10^{-07}
450	2.62×10^{-16}	7.56×10^{-14}	2.27×10^{-10}	8.09×10^{-09}	3.73×10^{-06}	1.33×10^{-04}
500	2.61×10^{-13}	3.95×10^{-11}	3.59×10^{-10}	8.37×10^{-09}	3.61×10^{-04}	8.40×10^{-03}
A	$1.88\times10^{+14}$	$9.18\times10^{+14}$	1.45×10^{-08}	1.05×10^{-08}	$1.96\times10^{+14}$	$1.42\times10^{+14}$
E_a	61.477	55.77	3.70	0.23	40.60	37.12

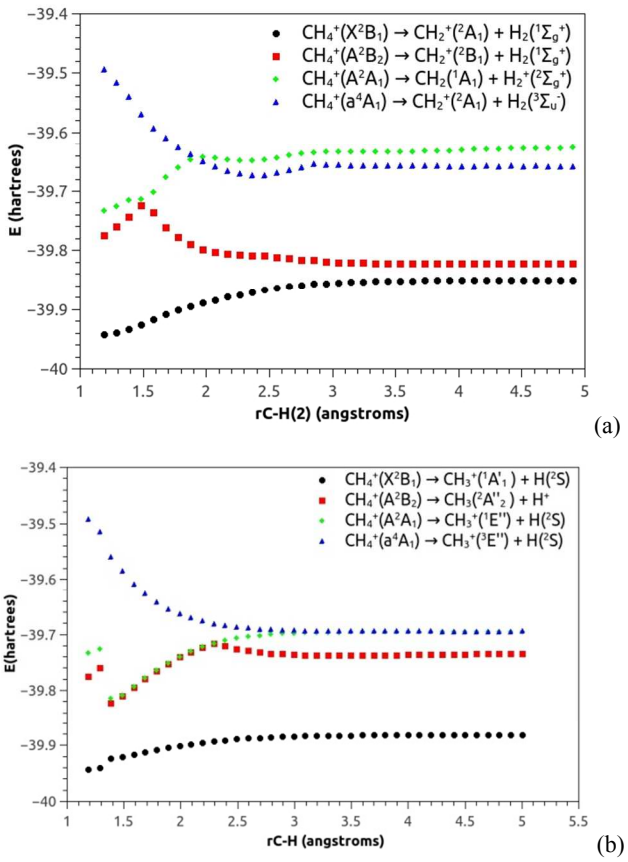

Fig. 3 Dissociation curves for the dissociation/recombination reactions at the MRCISD(7,8)/6-311G(d,p)//NEVPT2(7,8)/6-311G(2df,2pd) level; (a) reaction 1; (b) reactions 2 and 3.

Figure 3b shows that the first excited state does not influence CH_4^+ ground state dissociation (reaction 3). This result indicates that the jump discontinuity observed during the stretching of the C-(4) bond could be a consequence of the multiconfigurational method used to describe this reaction together with the contribution of high-energy configurations, such as |22012> and |22111>, to ground-state dissociation.

Previous studies have suggested that during the formation of CH_4^+ and related ions, high-order hydrocarbons can also be formed by polymerization induced by the presence of these ions[20,34,35]. A study by Fialkov[19] of the formation of various ions in flames and in combustion processes together with the results of the present study demonstrate that methane cation dissociation/recombination reactions can produce several ionic species in different electronic states if the correct amount of energy is furnished. However, analysis of several models available in the literature[10,54–63] revealed that ion-molecule reactions or ion-ion reactions were not taken into account. This may have been because of the low concentration of certain ions in the combustion process or the absence of kinetic data. The data obtained in the present study is therefore expected to be useful for testing combustion models.

Dissociation Kinetics

Table 4 shows the kinetic parameters at the high-pressure limit for dissociation/recombination reactions obtained for electronic energy calculated at the MRCISD(7,8)/6-311G(d,p)//NEVPT2(7,8)/6-311G(2df,2pd) level and harmonic vibrations and external moments of inertia calculated at the NEVPT2(7,8)/6-311G(2df,2pd) level. The kinetics study considers the dissociation of only the most stable configuration, the $\tilde{X}\ ^2B_1$ state. Rate coefficients were calculated in the range 273 K to 500 K, and the Arrhenius plots are shown in Figure 4. Rate coefficients for the recombination reaction (reaction 2) were determined from the relationship between equilibrium constant and forward and reverse reaction rate constants: $K = k_{for}/k_{rev}$.

A difference is observed between the CVTST and k_∞ rate coefficients. For reaction 1, the rate coefficients for the two methods differ by four orders of magnitude at lower temperatures but the differences lower at high temperatures. For reaction 3, the CVTST and k_∞ rate coefficients differ significantly at low temperatures, by three orders of magnitude at 273 K (Figure 4). For the temperature range investigated, the Arrhenius equation

does not exhibit curvilinear behavior for any of the reactions with either CVTST or k_∞, making the formulation of a generalized expression an unnecessary task.

The kinetic parameters and the analysis of the cumulative distribution of initial energies for an ensemble of methane cations indicate that the dissociation reaction proceeds only at high temperature, as in a combustion system, or if the molecules are formed with high energy, as in the radiolysis experiment. For these reasons, the k_∞ rate coefficients for all processes were determined at high temperatures (1000 K and 1500 K) (Table 5).

Table 5. High-pressure rate coefficients (k_∞) calculated at high temperatures. All dissociation reactions are in s^{-1} and the recombination reaction is in cm^3 $molecule^{-1}$ s^{-1}.

Temperature	Reaction 1	Reaction 2	Reaction 3
1000 K	$8.59\times10^{+01}$	1.14×10^{-08}	$9.74\times10^{+05}$
1500 K	$1.31\times10^{+06}$	1.54×10^{-08}	$4.28\times10^{+08}$

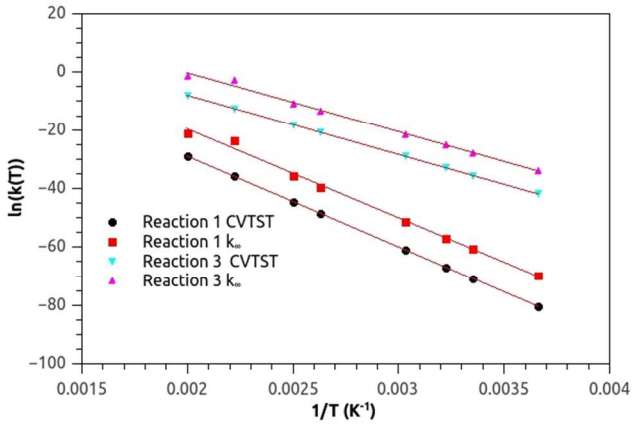

Fig. 4 Rate coefficients as a function of temperature. MRCISD(7,8)/6-311G(d,p)//NEVPT2(7,8)/6-311G(2df,2pd).

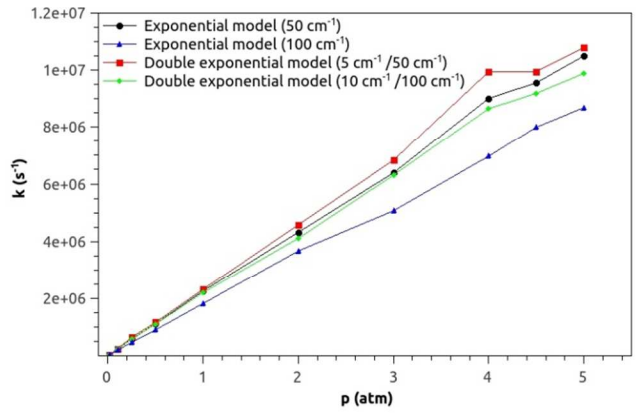

Fig. 5 Dependence of rate coefficients for reaction 3 on pressure fall-off for different forms of the energy transfer function and different α parameters. T = 1500 K.

The energy transfer function does not influence the rate coefficient at the high-pressure limit. However, in the pressure fall-off region, the unimolecular rate coefficients are strongly dependent on the energy transferred per impact and the mathematical model of the energy transfer function. Figure 5 shows the dependence of the rate coefficients on gas pressure for distinct α parameters and functional forms of the energy transfer function for reaction 3. At 1500 K in the pressure fall-off region, the rate coefficients are in the 2×10^4 to 2×10^7 s^{-1} range. There is agreement between the values determined with the exponential model for α = 50 cm^{-1} and those determined with the 0.1/10 bi-exponential model for α_2 = 100 cm^{-1}. There is good agreement between all collision models at low pressure values.

The fall-off rate coefficients increase monotonically with pressure and converge to the expected k_∞ value ($4.28\times10^{+08}$ s^{-1}) far above 5 atm.

In the range of temperatures studied, the Lennard-Jones collision rate coefficient varies from 2.95×10^{-10} to 3.48×10^{-10} cm^3 $molecule^{-1}$ s^{-1}. All thermally activated reactants are deactivated almost instantaneously when $\alpha \geq 300$ cm^{-1}. In the case of a CH_4^+ ensemble following a Boltzmann distribution, the strong collision assumption is valid when $\alpha > 300$ cm^{-1}. At the high-pressure limit and on the assumption that all collisions are strong, the first-order rate coefficient for deactivation is equal to the collision frequency[64]. Analyzing the increase in collision frequency as a function of pressure and temperature (Supplementary information section), it can be seen that the curves approach to a limit value at pressure values above to 5 atm. The collision frequency curves together with the fall-off curves indicate that for this system the high-pressure limit is reached at very high pressure, far above 5 atm.

CVTST and k_∞ rate coefficients were expected to be almost equal at the high-pressure limit. However, Figure 4 shows that this is not the case. This is because the CVTST coefficients were determined at 1.0 atm, and the high-pressure limit is reached far above 5 atm. As Table 4 shows, all the CVTST rate coefficients are lower than the k_∞ coefficients, proving that the former were not measured at the high-pressure limit. Formally, the called "CVTST" rate coefficient should be understood, and named, as a dissociation rate coefficient, since it were evaluated near to low pressure limit. However, the term CVTST rate coefficient will be preserved in order to clarify the method used to calculate the rate coefficient.

Further recombination reactions can be expected after dissociation through reaction 1. Using Dirichlet-type distributions, Plessis et al.[65] estimated the rate coefficient for the recombination reaction $CH_2^+ + H_2 \rightarrow CH_3^+ + H$ to be $1.2\times10^{+08}$ cm^3 $molecule^{-1}$ s^{-1}. After reaction 1, the products may recombine to form CH_3^+ ions in addition to those formed by reaction 3, the main dissociation channel. These coupled dissociation/recombination processes, which form new ionic species, will impact the ionic models used to describe the atmosphere of other planets and their moons[65].

Conclusions

The electronic structure and geometric parameters of CH_4^+ were analyzed, and a reactivity study using multiconfigurational methods was carried out for the dissociation/recombination processes for reactions 1-3. Kinetic parameters were determined using transition state theory and RRKM theory and by solving the master equation.

Methodological analysis showed that coupled cluster methods are not suitable for describing the dissociation/recombination of

CH_4^+; therefore, a complete multiconfigurational approach is required to take into account the wavefunction's multiconfigurational nature during bond-breaking, which is increased by the detachment of one binding electron.

The product distribution following dissociation of CH_4^+ is large. The major dissociation paths and their rate coefficients at the high-pressure limit are $CH_4^+(\tilde{X}\ ^2B_1) \rightarrow CH_3^+(A\ ^2A_1') + H(\ ^2S)$ (k(T) = $1.42\times10^{+14}$ s^{-1} exp(-37.12/RT)) and $CH_4^+(\tilde{X}\ ^2B_1) \rightarrow CH_2^+(A\ ^2A_1) + H_2(\ ^2\Sigma_g^+)$ (k(T) = $9.18\times10^{+14}$ s^{-1} exp(-55.77/RT)). The A^2B_2 and A^2A_1 excited states are inner-shell excited states and represent the electronic configuration of other ions formed after electron detachment from neutral methane. The dissociation curves corresponding to three excited states were determined and the electronic configuration of the products analyzed. All excited states are energetically substantially above the dissociation energies calculated for the CH_4^+ ground state. In the interstellar medium or in radiolysis experiments, the interaction of methane and related ions with high energy particles or radiation usually leads to the formation of several products: H_2 in different electronic states, H^+ CH_2^+ and others ions. In the interstellar medium, after irradiation of the surface of ices, the formation of various ions following methane cation dissociation is in general accompanied by the production of more complex hydrocarbons or other organic molecules if the target is in the presence of water or impurities[16,18,20,34,35]. These products are related to the family of ions formed after the irradiation of methane. An understanding of their structure and how they are produced depends on correctly identifying the ions, their structure and their electronic state, which this study sought to do. In flames, the high temperature induces ionization/dissociation of neutral methane and dissociation of CH_4^+, producing pollutants such as soot. We suggest that further studies be carried out to investigate the importance of the ion-neutral or ion-ion reactions described in this study for combustion kinetic models, since existing models generally include reactions involving free radicals and do not take into account reactions involving ions. The reactions analyzed here and kinetic parameters derived are expected to be useful for ionospheric models of planets and moons. The rate coefficients in the pressure fall-off region are expected to be of particular use as most processes in the interstellar medium occur at low pressure.

The collision parameters considered here are for neutral methane and were obtained from Miller[12]. For future kinetic studies, the Lennard-Jones parameters for the methane cation should be determined so that the influence of these parameters on rate coefficients, collision frequency and fall-off curves can be investigated.

Acknowledgments

The authors would like to thank CAPES, FAPERJ and CNPq for providing financial support and Professor Glauco Favilla Bauerfeldt at the *Universidade Federal Rural do Rio de Janeiro* for the helpful discussions he took part in.

(1) Lacy, J. H.; Carr, J. S.; J, N.; Evans, I.; Baas, F.; Achtermann, J. M.; Arens, J. F. *Astrophys. J.* **1991**, *376*, 556.
(2) Lindal, G. F.; Lyons, J. R.; Sweetnam, D. N.; Eshleman, V. R.; Hinson, D. P.; Tyler, G. L. *J. Geophys. Res.* **1987**, *92*, 14987.
(3) Owen, T. C.; Roush, T. L.; Cruikshank, D. P.; Elliot, J. L.; Young, L. A.; Bergh, C. de; Schmitt, B.; Geballe, T. R.; Brown, R. H.; Bartholomew, M. J. *Science* **1993**, *261*, 745–748.
(4) Brown, R. H.; Cruikshank, D. P.; Pendleton, Y.; Veeder, G. J. *Science* **1997**, *276*, 937–939.
(5) Cruikshank, D. P.; Roush, T. L.; Owen, T. C.; Geballe, T. R.; Bergh, C. de; Schmitt, B.; Brown, R. H.; Bartholomew, M. J. *Science* **1993**, *261*, 742–745.
(6) Schlesinger, B. *Nat. Gas* **1990**, *6*, 1–6.
(7) Moring, F. *Nat. Gas* **1999**, *15*, 27–29.
(8) Van Orden, A.; Saykally, R. J. *Chem. Rev.* **1998**, *98*, 2313–2358.
(9) Koinuma, H.; Horiuchi, T.; Inomata, K.; Ha, H.-K.; Nakajima, K.; Chaudhary, K. A. *Pure Appl. Chem.* **1996**, *68*, 1151–1154.
(10) Tsang, W.; Hampson, R. F. *J. Phys. Chem. Ref. Data* **1986**, *15*, 1087–1279.
(11) Davidson, D. F.; Hanson, R. K.; Bowman, C. T. *Int. J. Chem. Kinet.* **1995**, *27*, 305–308.
(12) Miller, J. A.; Klippenstein, S. J.; Raffy, C. *J. Phys. Chem.* **2002**, *106*, 4904–4913.
(13) Cobos, C. J.; Troe, J. *Z. für Phys. Chem.* **1990**, *167*, 129–149.
(14) Troe, J.; Ushakov, V. G. *J. Chem. Phys.* **2012**, *136*, 214309–214309 – 12–214309 – 214309–214312.
(15) Roueff, E.; Lique, F. Molecular Excitation in the Interstellar Medium: Recent Advances in Collisional, Radiative, and Chemical Processes. *Chemical Reviews*.
(16) Mejía, C. F.; Barros, A. L. F. de; Bordalo, V.; Silveira, E. F. da; Boduch, P.; Domaracka, A.; Rothard, H. *Mon. Not. R. Astron. Soc.* **2013**, *433*, 2368–2379.
(17) Barros, A. L. F. de; Bordalo, V.; Duarte, E. S.; Silveira, E. F. da; Domaracka, A.; Rothard, H.; Boduch, P. *Astron. & Astrophys.* **2011**, *531*.
(18) De Barros, A. L. F.; Bordalo, V.; Seperuelo Duarte, E.; F da Silveira, E.; Domaracka, A.; Rothard, H.; Boduch, P. *Astron. & Astrophys.* **2011**, *531*, A160–A160.
(19) Fialkov, A. B. *Prog. Energy Combust. Sci.* **1997**, *23*, 399–528.
(20) Rasul, G.; Prakash, G. K. S.; Olah, G. A. *Proc. Natl. Acad. Sci.* **10AD**, *94*, 11159–11162.
(21) Takeshita, K. *J. Chem. Phys.* **1987**, *86*, 329–338.
(22) Pauzat, F.; Ridard, J.; Levy, B. *Mol. Phys.* **1972**, *23*, 1163–1178.
(23) Mondal, T.; Varandas, A. J. C. *J. Chem. Phys.* **2011**, *135*, 174304–174304 – 9–174304 – 174304–174309.
(24) Potts, A. W.; Price, W. C.; Price, W. C. *Proc. R. Soc. London. A. Math. Phys. Sci.* **1972**, *326*, 165–179.
(25) Frey, R. F.; Davidson, E. R. *J. Chem. Phys.* **1988**, *88*, 1775–1785.
(26) Arents, J.; Allen, L. C. *J. Chem. Phys.* **1970**, *53*, 73–73.
(27) Paddon-Row, M. N.; Fox, D. J.; Pople, J. A.; Houk, K. N.; Pratt, D. W. *J. Am. Chem. Soc.* **1985**, *107*, 7696–7700.
(28) Zilberg, S.; Haas, Y. *J. Am. Chem. Soc.* **2003**, *125*, 1810–1820.
(29) Arents, J.; Allen, L. C. *J. Chem. Phys.* **2003**, *53*, 73–78.
(30) Wörner, H.; Veen, R. van der; Merkt, F. *Phys. Rev. Lett.* **2006**, *97*.
(31) Andrade, D. P. P.; Boechat-Roberty, H. M.; Martinez, R.; Homem, M. G. P.; da Silveira, E. F.; Rocco, M. L. M. *Surf. Sci.* **2009**, *603*, 1190–1196.
(32) Fernandez-Lima, F. A.; VilelaNeto, O. P.; Pimentel, A. S.; Ponciano, C. R.; Pacheco, M. A. C.; Nascimento, M. A. C.; Silveira, E. F. da. *J. Phys. Chem.* **2009**, *113*, 1813–1821.
(33) Collado, V. M.; Farenzena, L. S.; Ponciano, C. R.; Silveira, E. F. da; Wien, K. *Surf. Sci.* **2004**, *569*, 149–162.
(34) Sheridan, M. E.; Greer, E.; Libby, W. F. *J. Am. Chem. Soc.* **1972**, *94*, 2614–2618.
(35) Hamlet, P.; Moss, J.; Mittal, J. P.; Libby, W. F. *J. Am. Chem. Soc.* **1969**, *91*, 258–260.
(36) Angeli, C.; Cimiraglia, R.; Malrieu, J.-P. *Chem. Phys. Lett.* **2001**, *350*, 297–305.
(37) Dyall, K. G. *J. Chem. Phys.* **1995**, *102*, 4909–4918.
(38) Libint is a software stack for computing integrals used in molecular quantum mechanics and is used in ORCA package to compute two electrons integrals <http: //libint.valeyev.net>, **2013**.
(39) Neese, F. *Wiley Interdiscip. Rev. Comput. Mol. Sci.* **2012**, *2*, 73–78.
(40) MultiWell-2013 Software, Jan 2013, designed and maintained by J.R. Barker with contributors N.F. Ortiz, J.M. Preses, L.L. Lohr, A.

Maranzana, P.J. Stimac, T. L. Nguyen, and T. J. Dhilip Kumar, University of Michigan, Ann Arbor, MI; http://aoss.engin.umich.edu/multiwell/
(41) Barker, J. R. *Int. J. Chem. Kinet.* **2001**, *33*, 232–245.
(42) Robertson, S. H.; Pilling, M. J.; Jitariu, L. C.; Hillier, I. H. *Phys. Chem. Chem. Phys.* **2007**, *9*, 4085–4097.
(43) Dames, E. E.; Golden, D. M. *J. Phys. Chem.* **2013**.
(44) González-García, N.; Olzmann, M. *Phys. Chem. Chem. Phys.* **2010**, *12*, 12290–12290.
(45) Walsh, R.; Golden, D. M. *J. Phys. Chem.* **2008**, *112*, 3891–3897.
(46) Vereecken, L.; Peeters, J. *J. Phys. Chem.* **1999**, *103*, 5523–5533.
(47) Kuwata, K. T.; Kujala, B. J.; Morrow, Z. W.; Tonc, E. *Comput. Theor. Chem.* **2011**, *965*, 305–312.
(48) Nguyen, T. L.; Winterhalter, R.; Moortgat, G.; Kanawati, B.; Peeters, J.; Vereecken, L. *Phys. Chem. Chem. Phys.* **2009**, *11*, 4173–4183.
(49) Brown, N. J.; Miller, J. A. *J. Chem. Phys.* **1984**, *80*, 5568–5580.
(50) Maranzana, A.; Barker, J. R.; Tonachini, G. *J. Phys. Chem.* **2008**, *112*, 3666–3675.
(51) Barker, J. R.; Yoder, L. M.; King, K. D. *J. Phys. Chem.* **2001**, *105*, 796–809.
(52) Barker, J. R. *Int. J. Chem. Kinet.* **2009**, *41*, 748–763.
(53) Lyakh, D. I.; MusiaÅ,, M.; Lotrich, V. F.; Bartlett, R. J. *Chem. Rev.* **2011**.
(54) Wang, H.; Frenklach, M. *Combust. Flame* **1997**, *110*, 173–221.
(55) Dias, V.; Duynslaegher, C.; Contino, F.; Vandooren, J.; Jeanmart, H. *Combust. Flame* **2012**, *159*, 1814–1820.
(56) Diévart, P.; Won, S. H.; Dooley, S.; Dryer, F. L.; Ju, Y. *Combust. Flame* **2012**, *159*, 1793–1805.
(57) Rojas, A.; Barraza, J.; Barranco, R.; Lester, E. *Fuel* **2012**, *96*, 168–175.
(58) Baulch, D. L.; Cobos, C. J.; Cox, R. A.; Frank, P.; Hayman, G.; Just, T.; Kerr, J. A.; Murrells, T.; Pilling, M. J.; Troe, J.; Walker, R. W.; Warnatz, J. *J. Phys. Chem. Ref. Data* **1994**, *23*, 847–848.
(59) Westbrook, C. K.; Dryer, F. L. *Prog. Energy Combust. Sci.* **1984**, *10*, 1–57.
(60) Labecki, L.; Cairns, A.; Xia, J.; Megaritis, A.; Zhao, H.; Ganippa, L. C. *Appl. Energy* **2012**, *95*, 139–146.
(61) You, X.; Russi, T.; Packard, A.; Frenklach, M. *Proc. Combust. Inst.* **2011**, *33*, 509–516.
(62) Hoon Song, K.; Nag, P.; Litzinger, T. A.; Haworth, D. C. *Combust. Flame* **2003**, *135*, 341–349.
(63) Karwat, D. M. A.; Wagnon, S. W.; Wooldridge, M. S.; Westbrook, C. K. *J. Phys. Chem.* **2012**.
(64) Robinson, P. J.; Holbrook, K. A. *Unimolecular Reactions*; Wiley-Interscience, , **1972**, *cp 8*, pg 271.
(65) Plessis, S.; Carrasco, N.; Pernot, P. *J. Chem. Phys.* **2010**, *133*, 134110.